THE JOURNAL OF PHYSICAL CHEMISTRY Letters

Letter

Cite This: J. Phys. Chem. Lett. 2019, 10, 1394−1401

pubs.acs.org/JPCL

Plasmon Heating Promotes Ligand Reorganization on Single Gold Nanorods

Xiaoyu Cheng,[#,¶,†] Taryn P. Anthony,[#,†] Claire A. West,[‡] Zhongwei Hu,[‡] Vignesh Sundaresan,[#] Aaron J. McLeod,[#] David J. Masiello,[‡] and Katherine A. Willets*[,#]

[#]Department of Chemistry, Temple University, Philadelphia, Pennsylvania 19122, United States

[‡]Department of Chemistry, University of Washington, Seattle, Washington 98195, United States

Supporting Information

ABSTRACT: Single-molecule fluorescence microscopy is used to follow dynamic ligand reorganization on the surface of single plasmonic gold nanorods. Fluorescently labeled DNA is attached to gold nanorods via a gold−thiol bond using a low-pH loading method. No fluorescence activity is initially observed from the fluorescent labels on the nanorod surface, which we attribute to a collapsed geometry of DNA on the metal. Upon several minutes of laser illumination, a marked increase in fluorescence activity is observed, suggesting that the ligand shell reorganizes from a collapsed, quenched geometry to an upright, ordered geometry. The ligand reorganization is facilitated by plasmon-mediated photothermal heating, as verified by controls using an external heat source and simulated by coupled optical and heat diffusion modeling. Using super-resolution image reconstruction, we observe spatial variations in which ligand reorganization occurs at the single-particle level. The results suggest the possibility of nonuniform plasmonic heating, which would be hidden with traditional ensemble-averaged measurements.

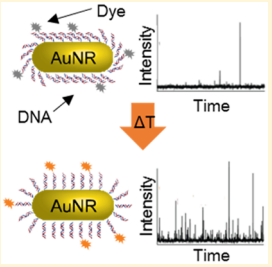

Plasmonic nanostructures exhibit unique optical features due to their ability to support localized surface plasmon resonance (LSPR), in which resonant incident electromagnetic radiation drives the surface conduction electrons to oscillate in phase.[1] Excitation at the LSPR generates significantly enhanced photon scattering (both intrinsic Rayleigh scattering from the nanostructure as well as Raman scattering from nearby analytes), photothermal heating, and hot charge carriers, all of which make plasmonic nanostructures promising for a range of applications, including optoelectronic devices, (bio)sensors, nanotherapeutics, and photothermal agents.[2,3] For many of these applications, it is typically necessary to functionalize the nanoparticle surfaces with organic ligands, which impart biocompatibility and target selectivity to allow delivery of therapeutic agents.[2,4,5] During the past 2 decades, remarkable progress has been made on optimizing surface modification strategies, allowing construction of increasingly more sophisticated nanointerfaces to reach molecular degrees of controls.[6−9] On the other hand, far less is known on how exactly ligands organize and behave on nanoparticle surfaces due to challenges in characterization, especially at the single-particle level where both electron and optical microscopy methods have limited contrast and/or spatial resolution.[9−12] That said, single-entity measurements are crucial because they enable rare events and heterogeneity within the sample to be studied, which are usually buried within the ensemble.[13] For instance, there is evidence to show that a single protein can initiate nanoparticle aggregation[14] and a single-molecule interaction can dominate plasmonic sensor responses.[15] The need for developing new characterization methods to study the ligand−particle interface at both the single-molecule and single-particle level has become increasingly evident.

We have previously shown that localization-based super-resolution imaging can address this challenge by localizing the position of single-ligand molecules attached to the surface of individual plasmonic gold nanorods (AuNRs), hence probing the ligand−particle interface with single-molecule sensitivity and <20 nm spatial resolution.[16−20] In localization-based super-resolution imaging, diffraction-limited emission from a single fluorescent molecule is fit to a model function (such as a 2-dimensional Gaussian) in order to extract the position of the emitter (see the SI for complete details of this process).[16,18] For samples in which multiple fluorophores are present at a density that renders them spatially unresolvable, the bulk of the emitters are shelved in a nonemissive "off" state, such that only one molecule is emitting at a time, enabling single-molecule localization. By toggling molecules between emissive ("on") and nonemissive ("off") states, each molecule within the sample can be uniquely localized.[21,22] Combining the positions of all localized emission events into a single plot creates a reconstructed image with spatial resolution that is at least an order of magnitude better than a far-field optical image (i.e., <20 nm vs >200 nm). In our previous work, double-stranded DNA (dsDNA) terminated with a thiol at the proximal end and a 5-carboxytetramethylrhodamine (TAMRA) fluorophore at the distal end, was attached to the surface of single AuNRs using a salt-loading protocol.[16,18] The position of each ligand

Received: January 10, 2019
Accepted: March 6, 2019
Published: March 6, 2019

DOI: 10.1021/acs.jpclett.9b00079
J. Phys. Chem. Lett. 2019, 10, 1394−1401

was localized by switching the TAMRA between emissive and nonemissive states using a triplet-mediated method.[16,18,23] The reconstructed images generated the correct shape and orientation of the nanorod by localizing the individual emitters on its surface but showed significant particle-to-particle heterogeneity in the apparent positions and density of the dsDNA ligands.[16,18−20]

Here, we use a different surface functionalization protocol in which the same thiolated dsDNA system is introduced to a AuNR solution under low pH conditions (see the SI for details).[24−26] Ensemble studies suggest that this functionalization strategy yields successful dsDNA loading on the AuNR surface;[25] however, our single-molecule studies show no characteristic fluorescence from the labeled dsDNA, suggesting that the ligands are initially collapsed on the surface, resulting in fluorescence quenching. The fluorescence is recoverable, however, through photothermal heating via plasmon excitation, indicating dynamic ligand rearrangement on the surface, which can be tracked in situ using super-resolution imaging. We also find that plasmon-driven ligand reorganization occurs in an apparent site-specific manner with significant particle-to-particle heterogeneity, suggesting the possibility of nonuniform plasmonic photothermal heating on the particle surface. These results are inaccessible using traditional ensemble-based methods, further supporting the need for in situ characterization tools that yield both single-particle and single-molecule sensitivity.

Figure 1A shows an intensity−time trace from a representative single AuNR, functionalized with TAMRA-labeled dsDNA using the low-pH loading protocol. To create this time trace, we integrate the fluorescence intensity

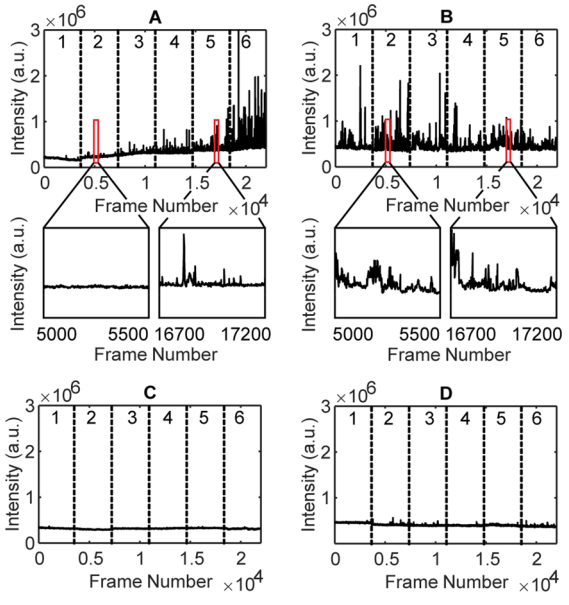

Figure 1. Representative single-molecule intensity vs time traces of single AuNRs. The dashed lines and numbers indicate the movie number in a sequential image stack. (A) AuNR modified with dye-labeled dsDNA using the low-pH loading method. (B) AuNR modified with dye-labeled dsDNA using the low-pH method and preheated in a 40 °C water bath for 10 min before observation. Insets show zoomed-in regions of the different time traces. (C) Bare AuNR with only CTAB surfactant present and (D) AuNR modified with dsDNA without fluorophore labels. Each movie contains 3650 frames with a 23 ms integration time.

associated with the single nanorod over six sequential image stacks (e.g., movies), consisting of 3650 frames each (we obtain the data as sequential movies rather a single continuous acquisition due to memory limitations of our computer). On the basis of our previous work,[16,18] we expect to observe strong bursts of fluorescence emission corresponding to individual TAMRA molecules transitioning between the emissive and nonemissive states. As Figure 1A shows, no fluorescence was observed during the first movie (section "1" of the plot), and only sporadic weak intensity fluorescence bursts were observed during movies 2−3. By movie 4, we observe increased fluorescence activity whose intensity and frequency grow over time. This time-dependent fluorescence response was unexpected as it was not observed in our previous work using the conventional salt-aging surface-modification method.[16,18] Because it is well-known that metals quench fluorescence when fluorophores are close to their surface (i.e., <5 nm),[27] we hypothesized that the dsDNA was initially collapsed on the gold, preventing the TAMRA label from emitting. Over time, the ligands rearrange on the surface, accessing a conformation that spaces the TAMRA dye sufficiently far from the metal to generate fluorescence activity. We hypothesize that this ligand reorganization is facilitated by photothermal heating of the gold nanoparticle due to plasmon excitation, which enables the ligands to overcome some activation barrier and reorient to a more upright, ordered geometry.

To test this hypothesis, we preheated our samples at 40 °C for 10 min (see the SI for details) before performing the single-molecule experiments. This temperature is easily accessible by laser heating of AuNRs[28] yet is below the melting temperature of the dsDNA used in these experiments ($T_m \approx 48$ °C). Figure 1B shows that with the heat pretreatment, single-molecule fluorescence activity is immediately detected from the beginning of the data acquisition, with activity and intensity comparable to what was observed in the sixth movie of the nonpretreated sample (Figure 1A, section 6). For comparison, nanorods coated with their native surfactant (cetyltrimethylammonium bromide, CTAB) and nanorods modified with dye-free dsDNA molecules did not show appreciable single-molecule activity throughout the observation (Figure 1C,D, respectively). These data provide additional evidence that heat is able to drive the ligand reorganization process, either provided by an external source or (in the case of the nonpretreated samples) through photothermal heating due to plasmon excitation.

To quantify the fluorescence behavior of the nanorods over time, we calculate the standard deviation of the fluorescence intensity for individual movies, as illustrated in Figure 2. The standard deviation is a useful metric for quantifying the gradual increase of fluorescence activity of the sample, as shown in the histograms in Figure 2 (panels B, D, and F), which map the distributions of fluorescence intensities associated with the single-molecule time traces in panels A, C, and E, respectively. In Figure 2A,B, the measured intensity largely originates from the luminescence background of the AuNR,[17,29,30] yielding tightly clustered intensity data in the histogram and a small standard deviation. As more fluorescence events are observed in later movies, excursions toward higher intensity are observed in the histograms, and this is reflected in increased standard deviation values. We find that this metric provides a simple handle for quantifying the transition from limited/no fluorescence activity to high activity without the need for deciding whether a molecule is "on" or "off" or isolating the

DOI: 10.1021/acs.jpclett.9b00079
J. Phys. Chem. Lett. 2019, 10, 1394−1401

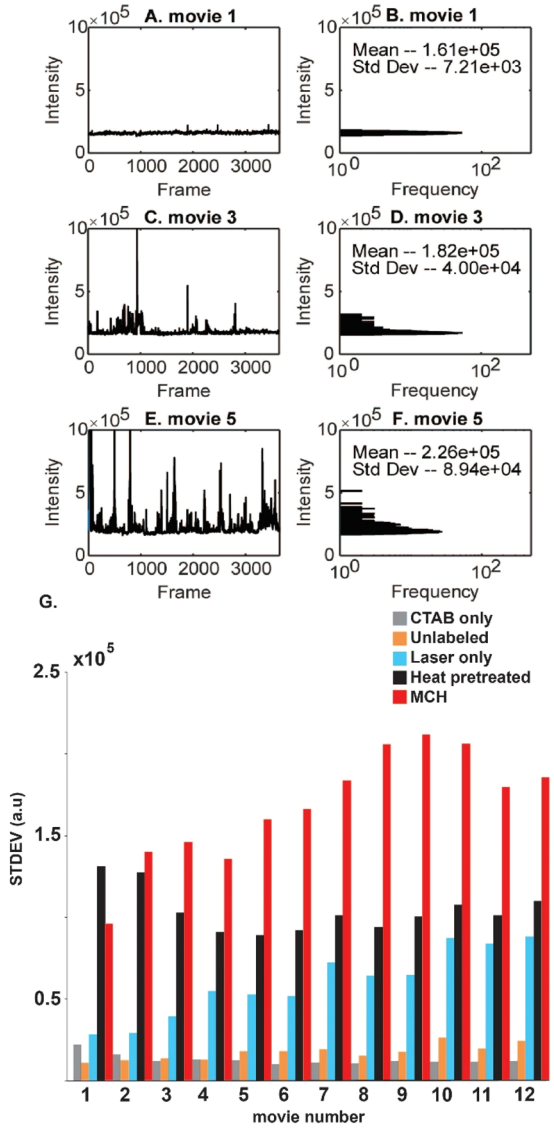

Figure 2. (A-F) (left column) Representative fluorescence intensity–time traces of a single nonheated AuNR modified with TAMRA-labeled dsDNA; (right column) corresponding histogram of the fluorescence intensity along with the calculated average and standard deviation of the distribution. The associated movie number is indicated in each plot. (G) Average standard deviation of the fluorescence intensity as a function of movie number (e.g., irradiation time) obtained from different nanorods for five different sample preparation protocols: (gray) as-prepared CTAB-coated AuNRs (21 particles), (orange) AuNRs functionalized with dsDNA without the TAMRA label (21 particles), (cyan) AuNRs functionalized with TAMRA-labeled dsDNA (31 particles), (black) AuNRs functionalized with TAMRA-labeled dsDNA and preheated at 40 °C for 10 min (22 particles), and (red) AuNRs functionalized with TAMRA-labeled dsDNA and incubated with MCH (37 particles).

molecular fluorescence from the gold luminescence (for example, during early movies, we observe several low-intensity events that cannot be easily discriminated above the noise floor of the measurement, making it difficult to absolutely assign the event as originating from a single molecule; moreover, fluctuations in the apparent background are also observed over time, which we attribute to fluctuations in the ligand shell during rearrangement that cannot be absolutely assigned as "on" or "off").

Figure 2G shows a plot of the average standard deviation in the fluorescence intensity as a function of movie number (e.g., irradiation time) for populations of nanorods prepared with five different surface functionalization treatments. The two control samples, representing the as-prepared CTAB-coated nanorods (gray bars) and the nanorods functionalized with dsDNA without the TAMRA label (orange bars), show low standard deviations in the measured signal that do not change over time, indicating that only stable luminescence from the gold is present in these samples. In comparison, the average standard deviation in the fluorescence from the TAMRA-labeled dsDNA samples without thermal pretreatment (shown in cyan) is similar to the control data for the first two movies but then shows a steady increase in the average standard deviation over time, indicating a ligand transition from a collapsed to a well-ordered state over the time scale of several minutes. Moreover, the average standard deviation rises to values that agree well with samples in which the TAMRA-labeled dsDNA-functionalized nanorods are subjected to a 10 min, 40 °C thermal pretreatment (black bars), further supporting the hypothesis that the transition is driven by plasmonic photothermal heating. Qualitatively, it appears that the standard deviation reaches a plateau after some period of time, suggesting that ligand reorganization has reached an equilibrium configuration, although both photobleaching and the possibility of multiple simultaneous emission events prevent a more quantitative analysis of this behavior. We also note that the ligand reorganization is irreversible as we do not observe a return to limited activity upon nanorod cooling (all imaging is done at room temperature). This indicates that the DNA is reaching a thermodynamically stable conformation, which is consistent with an equilibrium configuration associated with a well-packed monolayer, rather than a transient reconfiguration due to heat-induced DNA melting or gold–thiol bond cleavage.

Unsurprisingly, the standard deviations show large error bars (e.g., the standard deviation in our standard deviation values) when evaluated across a population of nanoparticles (see Figure S-6), indicating significant particle-to-particle heterogeneity, consistent with previous reports.[16,18,20,31] Ideally, we would study the kinetics of the transition as a function of laser intensity/wavelength (and thus heating power), but one challenge with our strategy for measuring laser-induced ligand reorganization is that the triplet-state photophysics of the dye (which determine our ability to toggle the dye between emissive and nonemissive states) is also linked to the laser intensity and excitation wavelength; thus, changing these parameters would affect the sensitivity of our single-molecule readout. To confirm that the transition is heat-mediated, however, we tested the response of the as-functionalized particles to a water bath at 30 °C and found that this temperature is insufficient to promote ligand reorganization after 10 min of heating (Figure S-7), suggesting a minimum threshold for driving the ligand transition.

To probe the range of temperatures accessible to the dsDNA bound to the surface, we performed coupled optical and steady-state heat diffusion modeling of the thermal near-field[32−34] (calculation details can be found in Figure S-8 caption text). The results indicate that laser-induced heating could raise local temperatures at the nanorod surface from 30 to as high as 90° above room temperature, depending on the thickness of the collapsed/upright DNA shell and the plasmon resonance of the nanorod (the simulations are based on a

DOI: 10.1021/acs.jpclett.9b00079
J. Phys. Chem. Lett. 2019, 10, 1394−1401

nanorod with length 74 nm and width 28 nm, which represents the mean value of the population). While this temperature range is above the melting temperature of the DNA used in these studies, our imaging experiments were performed under dry conditions with no solvent present into which the unattached DNA can diffuse, allowing continued association of the strands near the nanorod surface (see Figure S-9 for proposed surface configurations). Thus, simulation results confirm that plasmon-induced heating can easily generate sufficient temperature increases at the AuNR surface to drive the proposed ligand reorganization.

As a final check, we prepared TAMRA-labeled dsDNA-functionalized nanorods to which mercaptohexanol (MCH) was introduced after the dsDNA functionalization step (red bars in Figure 2G). MCH is known to intercalate between DNA strands on gold, resulting in molecules with a preferred orientation normal to the surface (Figure S-9D).[35,36] Similar to the preheated functionalized AuNRs, the MCH-treated nanorods exhibit more single-molecule fluorescence from the early stages of the observation (Figures S-22−S-24 and vide infra), although there is a still a time-dependent rise in the activity, suggesting that even with stabilizing ligands some surface rearrangement is possible.

Having shown that increases in the fluorescence activity of the TAMRA-labeled dsDNA over time are due to thermally driven ligand rearrangement from collapsed to upright ligand geometries, we next localize the spatial origin of the emission from the nonpretreated samples to determine how the ligand rearrangement proceeds both spatially and temporally. We note that the localization process has some inherent inaccuracy due to the coupling between the fluorophore and the plasmon modes of the nanorod, which is consistent with our previous studies;[16,37−40] however, this error tends to affect the absolute position of the emitter but not its relative position to some spatial fiducial (e.g., a molecule located on the left side of a horizontally oriented nanorod will almost always be localized to the left of the nanorod center). Thus, although our localization plots reflect the relative positions of the molecules on the AuNR surface, we expect them to provide reasonable insight into how the fluorescently labeled dsDNA is spatially distributed.

Figure 3 (panels A, C, and E) shows a series of scatter plots for three select movies associated with a single nanorod functionalized with TAMRA-labeled dsDNA with no thermal pretreatment (the complete data set is shown in Figure S-10). In the scatter plots, each point represents the peak of the fit of the diffraction-limited emission from a single emitter to a two-dimensional Gaussian. An "x" is shown at the position where the AuNR luminescence originates, providing a spatial fiducial that approximates the geometric center of the nanorod.[17,18] The data shows that during the ligand reorganization process the time-dependent fluorescence activity does not mirror the underlying shape of the nanorods but rather appears localized to clusters. For example, in movie 4 (Figure 3A), most of the fluorescent events are clustered to the upper left of the nanorod center, while in movie 9 (Figure 3C), the cluster of events has shifted to the lower right. Over time, as more molecules become active, the fluorescence is localized to multiple regions of the AuNR (Figure 3E, movie 11). The clustering of the activity in the early data suggests that some element of cooperativity may be present, such that the reorientation of dsDNA in one region of the nanorod promotes subsequent organization of its neighbors. However,

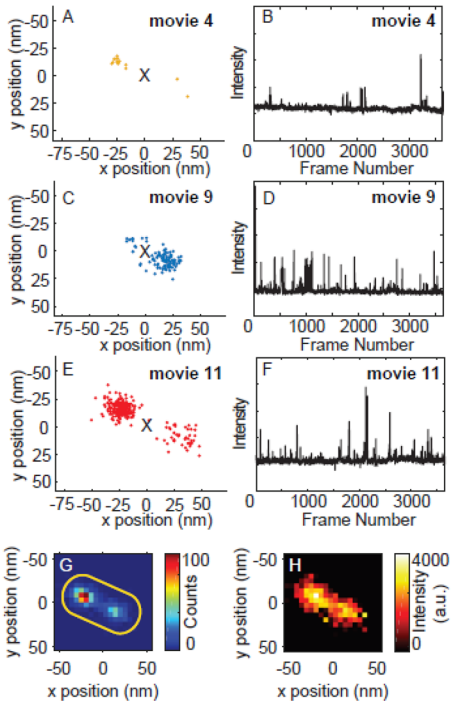

Figure 3. (A−F) Super-resolution reconstructed images (left column) and associated time traces (right column) for a TAMRA-dsDNA-labeled AuNR. An "x" is shown in the reconstructed images at (0,0), which indicates the spatial origin of the gold luminescence and the geometric center of the AuNR. Data from three different movies are shown, as indicated. (G) Spatial frequency histogram showing the frequency with which the TAMRA emission is localized at a particular region in space. The image includes data from 11 movies. A gold oval indicates the expected size and orientation of the AuNR. (H) Intensity histogram showing the average intensity of the TAMRA emission for each bin of the histogram shown in (G).

we note that it is not possible to distinguish multiple molecules emitting within the same general location from a single molecule turning on multiple times;[41] therefore, we cannot definitively attribute the clustering behavior to cooperativity effects.

Figure 3G shows the final reconstructed image, summing the activity over 12 movies and plotting the localization data in histogram form (the average intensity observed at the different positions is also included as Figure 3H). The final reconstructed image shows that more events are localized at the ends of the nanorod, suggesting either (1) preferential dsDNA binding near the ends or (2) preferential ligand reorganization near the ends. Previous super-resolution imaging work from our lab has shown that preferential dsDNA binding can occur on the ends of nanorods, believed to be due to the increased curvature at the ends that allows for improved penetration of the CTAB bilayer.[16,18,20,42] Figure 4, left column, shows additional examples of AuNRs functionalized with TAMRA-labeled dsDNA with no thermal pretreatment (complete data sets are shown in Figures S-11−S-16), in which similar spatially dependent clustering of fluorescent events is observed near the ends of the nanorods in the final reconstructed images, with limited activity in the center. For comparison, Figure 4, right column (full data sets in Figures S-17−S-21) shows examples of AuNRs that were preheated at 40 °C for 10 min before analysis, and the fluorescence in the final reconstructed images is observed to be more uniformly

DOI: 10.1021/acs.jpclett.9b00079
J. Phys. Chem. Lett. 2019, 10, 1394−1401

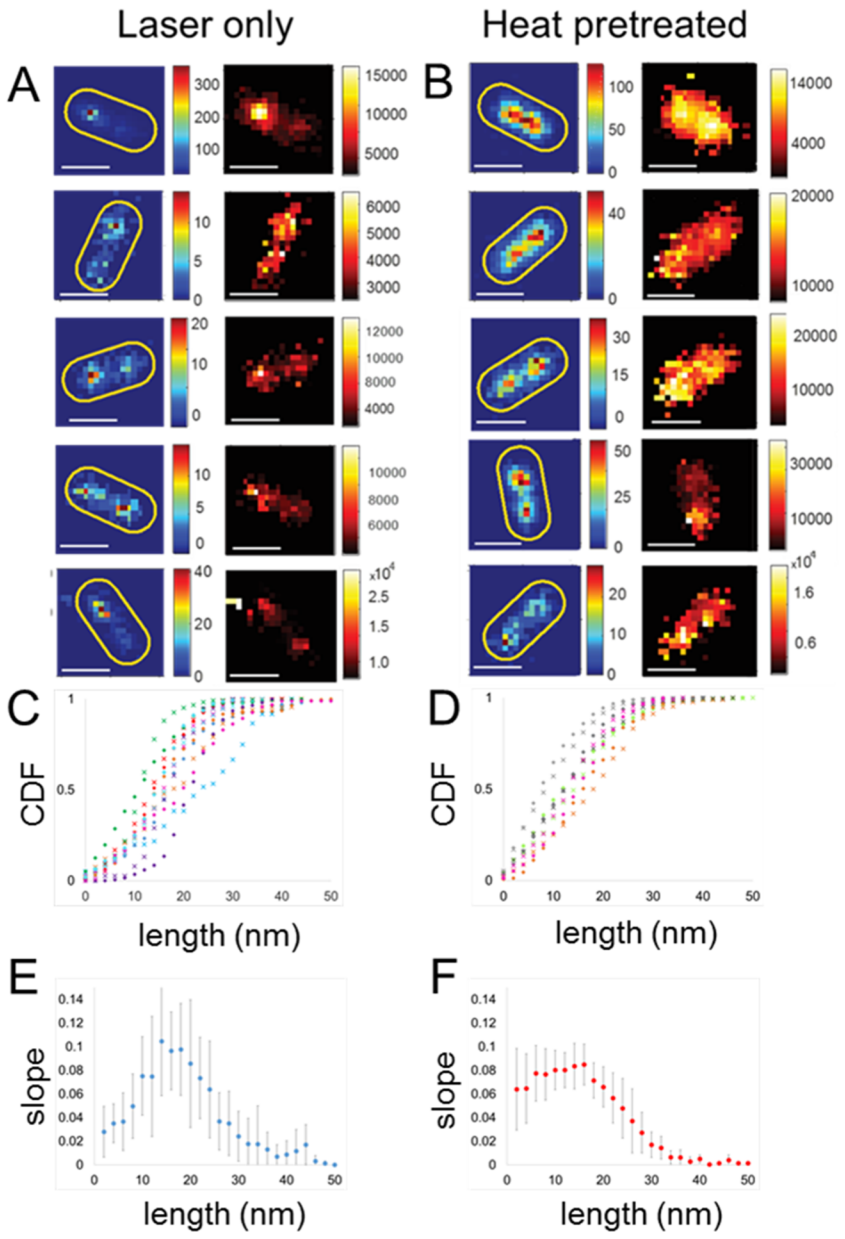

Figure 4. (A,B) Spatial frequency histograms (blue color maps) and intensity histograms (orange color maps) associated with (A) laser-only illuminated samples and (B) heat pretreated samples. The gold ovals indicate the expected size and orientation of each AuNR. The scale bars are 50 nm. (C,D) Cumulative distribution function plots associated with (C) laser-only illuminated samples and (D) heat pretreated samples. Data points are shown as filled circles and "x" to indicate data either positive or negative of the nanorod center. The color scheme associated with individual rods is shown in Figure S-25. (E,F) Averaged first derivative of the CDF plots associated with the (E) laser-only illuminated and (F) heat pretreated samples. Error bars are the standard deviation.

localized over the length of the nanorod, although some heterogeneity is still observed (particularly, the bottom two examples).

To quantify the difference in observed behaviors, we calculate the cumulative distribution function (CDF), which describes the probability of finding fluorescence activity at some distance from the center of the nanorod.[18] For this analysis, we rotate each nanorod along its length dimension, such that the nanorod is oriented along the *x*-axis, and then determine the number of points that fall within a certain distance either to the right (positive) or to the left (negative) of the nanorod center along the length dimension. The results of the CDF analysis are shown for both the case where the samples were only illuminated by the laser (Figure 4C) and the samples that were preheated at 40 °C (Figure 4D). From our previous work, we expect a linear rise in the CDF from the center to roughly half of the distance to the end of the nanorod (here, ∼20 nm) for uniformly functionalized rods.[18] To test whether our samples show this ideal behavior, we calculate the first derivative of the CDF plots (Figure S-25). Figure 4E,F shows the average slope of the CDF plots as a function of distance for both the laser-heated and thermally pretreated samples, respectively. A clear difference is observed between the two sample types: while the average slope of the CDF plot for the thermally pretreated samples is roughly constant over ∼20 nm, indicating a linear rise in the CDF (Figure 4F), the slope consistently changes over the length of the nanorod for the samples that were only exposed to the laser (Figure 4E).

DOI: 10.1021/acs.jpclett.9b00079
J. Phys. Chem. Lett. 2019, 10, 1394−1401

The former behavior is consistent with uniformly functionalized nanorods, suggesting that the dsDNA tends to reorient to an upright position across the nanorod surface when exposed to an external heat source. On the other hand, the latter behavior reveals that the CDF distributions tend to be sigmoidal, rather than linear, due to a dearth of fluorescence events near the center of the nanorod, suggesting spatial variations in ligand reorganization in plasmonically heated samples. These data suggest that we are observing spatial differences between ligand reorganization when we use plasmon excitation versus when we apply an external heat source that cannot be explained by local curvature effects alone.

To understand how plasmon excitation can produce spatial variations in ligand rearrangement across the nanorod surface, we simulated the spatially dependent thermal profile at the nanorod surface, as shown in Figure S-8. The results indicate that the thermal environment of the DNA depends on its position on the nanorod surface, particularly with respect to the substrate, which serves as a heat sink in the plasmonic heating experiments (in contrast to the externally heated samples, where both the AuNRs and the substrate are at elevated temperatures). Thus, we expect that the higher local temperature at the top and ends of the nanorod would induce a higher extent of thermally driven rearrangement in DNA located along these regions of the nanorods than that in DNA located closer to the substrate. Given that the super-resolution data shown in Figures 3 and 4 are two-dimensional projections of a three-dimensional system, it is impossible to know whether we are more sensitive to ligands near the substrate rather than the top of the nanorod, which would explain our results. Calculations are in progress to understand how the substrate affects collected fluorescence from these highly coupled systems. Beyond the role of the substrate, previous work has reported higher local heating at the ends of gold nanowires, which was ascribed to the reduced ability of the nanowires to dissipate heat at the ends.[43] Thus, we hypothesize that the spatially confined nature of plasmon heating and its ability to transfer that heat into the environment induces spatial asymmetry in the local temperature profiles, generating spatial heterogeneity in the reconstructed images. We note that other effects may also be in play, such as ligand motion on the surface or hot electron effects, although it is difficult to see how ligand motion would induce asymmetry in the reconstructed images. Hot electrons, on the other hand, can interact with surface-bound DNA in spatially heterogeneous ways, although work from Halas and co-workers has shown that this effect is minimal in comparison to photothermal heating for nanorod substrates.[44]

Even with the improved spatial homogeneity associated with external heating, there remains some degree of nonuniform spatial localization in the fluorescence activity (Figure 4B, bottom panels), suggesting that the original DNA binding to the surface is not completely homogeneous. As discussed earlier, the curvature at the ends of the rod allows more conformational flexibility, and this may be reflected in more reorganization occurring at these sites.[45] We have also noted this behavior in our previous work, with respect to not only the spatial localization of the signals but also the variation in the number of fluorescent events observed.[18] We attribute the latter effect to statistical differences in the number of labeled vs unlabeled DNA molecules that bind to each nanorod surface, based on our previous work showing that the average fluorescence activity scales with the dilution factor of the labeled dsDNA.[18] Moreover, reconstructed images of MCH-promoted AuNRs (Figures S-22−S-24) also show enhanced localization activity near the ends in the final reconstructed images, consistent with intercalation favoring the ends of the nanorod. This result highlights the importance of single-nanoparticle experiments because they reveal heterogeneity across a population that would be otherwise hidden in an ensemble-averaged measurement.

To conclude, we demonstrate the use of far-field single-molecule super-resolution microscopy for the detection of dynamic reorganization behavior of DNA self-assembled monolayers on single-plasmonic AuNRs. As-prepared functionalized nanorods do not show fluorescence activity, indicating ligand collapse on the surface; however, ligands can undergo a conformational shift toward an upright geometry by plasmon-induced photothermal heating, external heating, or the introduction of an intercalating ligand such as MCH. We also show that ligand reorganization is highly temporally and spatially heterogeneous across the nanorod surface and across different particles, with signatures of site-specific reorganization. This study enables new opportunities for probing surface processes on single nanostructures using optical imaging with subdiffraction resolution, revealing interfacial dynamics inaccessible with ensemble measurements. Future work will focus on how the density and properties of the DNA linker affect ligand reorganization, probe how the nanoparticle shape, size, and environment impact the ability to both generate and locally dissipate heat, and attempt to measure quantitative temperatures at nanoparticle surfaces, with the ultimate goal of understanding how local heating effects can be controlled at the nanoscale.

■ ASSOCIATED CONTENT

Supporting Information

The Supporting Information is available free of charge on the ACS Publications website at DOI: 10.1021/acs.jpclett.9b00079.

Sample preparation, experimental setup, analysis procedure, nanorod characterization, simulation details, and complete single-molecule super-resolution imaging data sets (PDF)

■ AUTHOR INFORMATION

Corresponding Author

*E-mail: kwillets@temple.edu.

ORCID

Xiaoyu Cheng: 0000-0003-0901-8496
Taryn P. Anthony: 0000-0002-5517-2999
Zhongwei Hu: 0000-0002-2783-7981
Vignesh Sundaresan: 0000-0001-9390-1681
Aaron J. McLeod: 0000-0002-3720-0992
David J. Masiello: 0000-0002-1187-0920
Katherine A. Willets: 0000-0002-1417-4656

Present Address

[¶]National Engineering Research Center for Optical Instruments, State Key Laboratory of Modern Optical Instrumentation, College of Optical Science and Engineering, Zhejiang University, Hangzhou 310058, China.

Author Contributions

[†]X.C. and T.A. contributed equally to this work.

DOI: 10.1021/acs.jpclett.9b00079
J. Phys. Chem. Lett. 2019, 10, 1394−1401

Notes

The authors declare no competing financial interest.

■ ACKNOWLEDGMENTS

This work was supported by the United States National Science Foundation under Grants CHE-1540927 (K.A.W.), CHE-1728340 (K.A.W.), and CHE-1727092 (D.J.M.). A.J.M. acknowledges support from the Temple University Diamond Research Scholars. D.J.M. acknowledges additional support from the University of Washington through the use of advanced computational, storage, and networking infrastructure provided by the Hyak supercomputer system at the University of Washington.

■ REFERENCES

(1) Halas, N. J.; Lal, S.; Chang, W.-S.; Link, S.; Nordlander, P. Plasmons in Strongly Coupled Metallic Nanostructures. *Chem. Rev.* **2011**, *111*, 3913−3961.
(2) Rosi, N. L.; Mirkin, C. A. Nanostructures in Biodiagnostics. *Chem. Rev.* **2005**, *105*, 1547−1562.
(3) Mayer, K. M.; Hafner, J. H. Localized Surface Plasmon Resonance Sensors. *Chem. Rev.* **2011**, *111*, 3828−3857.
(4) Love, J. C.; Estroff, L. A.; Kriebel, J. K.; Nuzzo, R. G.; Whitesides, G. M. Self-Assembled Monolayers of Thiolates on Metals as a Form of Nanotechnology. *Chem. Rev.* **2005**, *105*, 1103−1170.
(5) Elghanian, R.; Storhoff, J. J.; Mucic, R. C.; Letsinger, R. L.; Mirkin, C. A. Selective Colorimetric Detection of Polynucleotides Based on the Distance-Dependent Optical Properties of Gold Nanoparticles. *Science* **1997**, *277*, 1078−1081.
(6) Gooding, J. J.; Ciampi, S. The Molecular Level Modification of Surfaces: from Self-assembled Monolayers to Complex Molecular Assemblies. *Chem. Soc. Rev.* **2011**, *40*, 2704−18.
(7) Cheng, X.; Lowe, S. B.; Reece, P. J.; Gooding, J. J. Colloidal Silicon Quantum Dots: from Preparation to the Modification of Self-Assembled Monolayers (SAMs) for Bio-applications. *Chem. Soc. Rev.* **2014**, *43*, 2680−700.
(8) Casalini, S.; Bortolotti, C. A.; Leonardi, F.; Biscarini, F. Self-assembled Monolayers in Organic Electronics. *Chem. Soc. Rev.* **2017**, *46*, 40−71.
(9) Cheng, X.; Lowe, S. B.; Ciampi, S.; Magenau, A.; Gaus, K.; Reece, P. J.; Gooding, J. J. Versatile "Click Chemistry" Approach to Functionalizing Silicon Quantum Dots: Applications Toward Fluorescent Cellular Imaging. *Langmuir* **2014**, *30*, 5209−16.
(10) Chen, T.; Dong, B.; Chen, K.; Zhao, F.; Cheng, X.; Ma, C.; Lee, S.; Zhang, P.; Kang, S. H.; Ha, J. W.; Xu, W.; Fang, N. Optical Super-Resolution Imaging of Surface Reactions. *Chem. Rev.* **2017**, *117*, 7510−7537.
(11) Hauser, M.; Wojcik, M.; Kim, D.; Mahmoudi, M.; Li, W.; Xu, K. Correlative Super-Resolution Microscopy: New Dimensions and New Opportunities. *Chem. Rev.* **2017**, *117*, 7428−7456.
(12) Cheng, X.; Hinde, E.; Owen, D. M.; Lowe, S. B.; Reece, P. J.; Gaus, K.; Gooding, J. J. Enhancing Quantum Dots for Bioimaging using Advanced Surface Chemistry and Advanced Optical Microscopy: Application to Silicon Quantum Dots (SiQDs). *Adv. Mater.* **2015**, *27*, 6144−50.
(13) Dickson, R. M.; Cubitt, A. B.; Tsien, R. Y.; Moerner, W. E. On/off Blinking and Switching Behaviour of Single Molecules of Green Fluorescent Protein. *Nature* **1997**, *388*, 355.
(14) Dominguez-Medina, S.; Kisley, L.; Tauzin, L. J.; Hoggard, A.; Shuang, B.; D. S. Indrasekara, A. S.; Chen, S.; Wang, L.-Y.; Derry, P. J.; Liopo, A.; Zubarev, E. R.; Landes, C. F.; Link, S. Adsorption and Unfolding of a Single Protein Triggers Nanoparticle Aggregation. *ACS Nano* **2016**, *10*, 2103−2112.
(15) Taylor, A. B.; Zijlstra, P. Single-Molecule Plasmon Sensing: Current Status and Future Prospects. *ACS Sens.* **2017**, *2*, 1103−1122.
(16) Blythe, K. L.; Willets, K. A. Super-Resolution Imaging of Fluorophore-Labeled DNA Bound to Gold Nanoparticles: A Single-Molecule, Single-Particle Approach. *J. Phys. Chem. C* **2016**, *120*, 803−815.
(17) Titus, E. J.; Willets, K. A. Accuracy of Superlocalization Imaging Using Gaussian and Dipole Emission Point-Spread Functions for Modeling Gold Nanorod Luminescence. *ACS Nano* **2013**, *7*, 6258−6267.
(18) Blythe, K. L.; Titus, E. J.; Willets, K. A. Effects of Tuning Fluorophore Density, Identity, and Spacing on Reconstructed Images in Super-Resolution Imaging of Fluorophore-Labeled Gold Nanorods. *J. Phys. Chem. C* **2015**, *119*, 28099−28110.
(19) Blythe, K. L.; Mayer, K. M.; Weber, M. L.; Willets, K. A. Ground State Depletion Microscopy for Imaging Interactions Between Gold Nanowires and Fluorophore-labeled Ligands. *Phys. Chem. Chem. Phys.* **2013**, *15*, 4136−4145.
(20) Blythe, K. L.; Titus, E. J.; Willets, K. A. Triplet-State-Mediated Super-Resolution Imaging of Fluorophore-Labeled Gold Nanorods. *ChemPhysChem* **2014**, *15*, 784−793.
(21) Betzig, E.; Patterson, G. H.; Sougrat, R.; Lindwasser, O. W.; Olenych, S.; Bonifacino, J. S.; Davidson, M. W.; Lippincott-Schwartz, J.; Hess, H. F. Imaging Intracellular Fluorescent Proteins at Nanometer Resolution. *Science* **2006**, *313*, 1642−1645.
(22) Rust, M. J.; Bates, M.; Zhuang, X. Sub-diffraction-limit Imaging by Stochastic Optical Reconstruction Microscopy (STORM). *Nat. Methods* **2006**, *3*, 793−5.
(23) Fölling, J.; Bossi, M.; Bock, H.; Medda, R.; Wurm, C. A.; Hein, B.; Jakobs, S.; Eggeling, C.; Hell, S. W. Fluorescence Nanoscopy by Ground-state Depletion and Single-molecule Return. *Nat. Methods* **2008**, *5*, 943.
(24) Zhang, X.; Servos, M. R.; Liu, J. Instantaneous and Quantitative Functionalization of Gold Nanoparticles with Thiolated DNA Using a pH-Assisted and Surfactant-Free Route. *J. Am. Chem. Soc.* **2012**, *134*, 7266−7269.
(25) Shi, D.; Song, C.; Jiang, Q.; Wang, Z.-G.; Ding, B. A Facile and Efficient Method to Modify Gold Nanorods with Thiolated DNA at a Low pH Value. *Chem. Commun.* **2013**, *49*, 2533−2535.
(26) Baaske, M. D.; Foreman, M. R.; Vollmer, F. Single-molecule Nucleic Acid Interactions Monitored on a Label-free Microcavity Biosensor Platform. *Nat. Nanotechnol.* **2014**, *9*, 933−939.
(27) Tam, F.; Goodrich, G. P.; Johnson, B. R.; Halas, N. J. Plasmonic Enhancement of Molecular Fluorescence. *Nano Lett.* **2007**, *7*, 496−501.
(28) Carattino, A.; Caldarola, M.; Orrit, M. Gold Nanoparticles as Absolute Nanothermometers. *Nano Lett.* **2018**, *18*, 874−880.
(29) Mertens, J.; Kleemann, M.-E.; Chikkaraddy, R.; Narang, P.; Baumberg, J. J. How Light Is Emitted by Plasmonic Metals. *Nano Lett.* **2017**, *17*, 2568−2574.
(30) Link, S.; El-Sayed, M. A. Spectral Properties and Relaxation Dynamics of Surface Plasmon Electronic Oscillations in Gold and Silver Nanodots and Nanorods. *J. Phys. Chem. B* **1999**, *103*, 8410−8426.
(31) Sambur, J. B.; Chen, T.-Y.; Choudhary, E.; Chen, G.; Nissen, E. J.; Thomas, E. M.; Zou, N.; Chen, P. Sub-particle Reaction and Photocurrent Mapping to Optimize Catalyst-modified Photoanodes. *Nature* **2016**, *530*, 77−80.
(32) Purcell, E. M.; Pennypacker, C. R. Scattering and Absorption of Light by Nonspherical Dielectric Grains. *Astrophys. J.* **1973**, *186*, 705−714.
(33) Draine, B. T.; Flatau, P. J. Discrete-Dipole Approximation For Scattering Calculations. *J. Opt. Soc. Am. A* **1994**, *11*, 1491−1499.
(34) Baldwin, C. L.; Bigelow, N. W.; Masiello, D. J. Thermal Signatures of Plasmonic Fano Interferences: Toward the Achievement of Nanolocalized Temperature Manipulation. *J. Phys. Chem. Lett.* **2014**, *5*, 1347−1354.
(35) Herne, T. M.; Tarlov, M. J. Characterization of DNA Probes Immobilized on Gold Surfaces. *J. Am. Chem. Soc.* **1997**, *119*, 8916−8920.
(36) Levicky, R.; Herne, T. M.; Tarlov, M. J.; Satija, S. K. Using Self-Assembly to Control the Structure of DNA Monolayers on Gold: A Neutron Reflectivity Study. *J. Am. Chem. Soc.* **1998**, *120*, 9787−9792.

DOI: 10.1021/acs.jpclett.9b00079
J. Phys. Chem. Lett. 2019, 10, 1394−1401

(37) Wertz, E.; Isaacoff, B. P.; Flynn, J. D.; Biteen, J. S. Single-Molecule Super-Resolution Microscopy Reveals How Light Couples to a Plasmonic Nanoantenna on the Nanometer Scale. *Nano Lett.* **2015**, *15*, 2662−2670.
(38) Willets, K. A.; Wilson, A. J.; Sundaresan, V.; Joshi, P. B. Super-Resolution Imaging and Plasmonics. *Chem. Rev.* **2017**, *117*, 7538−7582.
(39) Su, L.; Yuan, H.; Lu, G.; Rocha, S.; Orrit, M.; Hofkens, J.; Uji-i, H. Super-resolution Localization and Defocused Fluorescence Microscopy on Resonantly Coupled Single-Molecule, Single-Nanorod Hybrids. *ACS Nano* **2016**, *10*, 2455−2466.
(40) Heaps, C. W.; Schatz, G. C. Modeling Super-resolution SERS Using a T-matrix Method to Elucidate Molecule-nanoparticle Coupling and the Origins of Localization Errors. *J. Chem. Phys.* **2017**, *146*, 224201.
(41) Thompson, M. A.; Lew, M. D.; Moerner, W. E. Extending Microscopic Resolution with Single-molecule Imaging and Active Control. *Annu. Rev. Biophys.* **2012**, *41*, 321−42.
(42) Burrows, N. D.; Lin, W.; Hinman, J. G.; Dennison, J. M.; Vartanian, A. M.; Abadeer, N. S.; Grzincic, E. M.; Jacob, L. M.; Li, J.; Murphy, C. J. Surface Chemistry of Gold Nanorods. *Langmuir* **2016**, *32*, 9905−9921.
(43) Carlson, M. T.; Green, A. J.; Khan, A.; Richardson, H. H. Optical Measurement of Thermal Conductivity and Absorption Cross-Section of Gold Nanowires. *J. Phys. Chem. C* **2012**, *116*, 8798−8803.
(44) Huschka, R.; Zuloaga, J.; Knight, M. W.; Brown, L. V.; Nordlander, P.; Halas, N. J. Light-Induced Release of DNA from Gold Nanoparticles: Nanoshells and Nanorods. *J. Am. Chem. Soc.* **2011**, *133*, 12247−12255.
(45) Hinman, J. G.; Eller, J. R.; Lin, W.; Li, J.; Li, J.; Murphy, C. J. Oxidation State of Capping Agent Affects Spatial Reactivity on Gold Nanorods. *J. Am. Chem. Soc.* **2017**, *139*, 9851−9854.

DOI: 10.1021/acs.jpclett.9b00079
J. Phys. Chem. Lett. 2019, 10, 1394−1401